Mesoscopic model for dynamic simulations of carbon nanotubes

Leonid V. Zhigilei*
University of Virginia, Department of Materials Science and Engineering, 116 Engineer's Way, Charlottesville, Virginia 22904-4745 USA

Chenyu Wei† and Deepak Srivastava‡
Computational Nanotechnology, NASA Ames Research Center, Mail Stop 229-1, Moffett Field, California 94035-1000 USA
(Received 21 August 2004; revised manuscript received 5 November 2004; published 14 April 2005)

A mesoscopic model is developed for static and dynamic simulations of nanomechanics of carbon nanotubes (CNTs). The model is based on a coarse-grained representation of CNTs as "breathing flexible cylinders" consisting of a variable number of segments. Internal interactions within a CNT are described by a mesoscopic force field designed and parameterized based on the results of atomic-level molecular dynamics simulations. The radial size of the CNTs and external interactions among multiple CNTs and molecular matrix are introduced through a computationally efficient "virtual surface" method that does not require explicit representation of the CNT's surfaces. The mesoscopic model is shown to reproduce well the dynamic behavior of individual CNTs predicted in atomistic simulations at a minor fraction of the computational cost.

DOI: 10.1103/PhysRevB.71.165417 PACS number(s): 61.46.+w, 62.30.+d, 02.70.Ns

I. INTRODUCTION

Since their discovery in 1991,[1] both single- and multiwalled carbon nanotubes (CNTs) have been investigated rigorously for their excellent mechanical and physical properties at a very low density. Recent reviews summarize theoretical and experimental results on the nanomechanics, and on the chemical and electronic properties of CNTs.[2–7] From the mechanical characteristics viewpoint, the high aspect ratio, high stiffness, flexibility, and strength of CNTs suggest that they can be considered as ideal reinforcing nanofibers in nanotube-matrix composites.[8]

Despite the great interest in the mechanical and physical properties of CNTs and CNT-based nanocomposites, there have been no computational studies addressing the dynamic behavior of multiple CNTs in a matrix. Computational efforts have been largely limited to quasistatic molecular dynamics (MD) simulations of individual nanotubes, either isolated[9–11] or surrounded by polymer molecules.[12–15] Although investigation of the mechanical properties of individual nanotubes and adhesion between nanotubes and polymer matrix are necessary elements in the analysis of the mechanical behavior of nanocomposites, the processes of plastic deformation and fracture of nanocomposite materials can have complex collective character that cannot be derived directly from the properties of individual components and can only be addressed in simulations performed at the length scales characteristic of multiple interacting nanotubes; i.e., at a mesoscopic level.

Dynamic simulations of the nanomechanics of multiwalled nanotubes, bundles of single-walled nanotubes, single-walled nanotubes in continuously spun fibers, and nanotubes in polymer composites have been hindered by the absence of appropriate mesoscopic models. For CNTs, the descriptions originating from continuum mechanics, e.g., elastic shell or beam models have been proposed,[16–20] and critically reviewed in Ref. 21. While the analogy with macroscopic beams and shells can provide a convenient tool for analysis and description of the mechanical properties of CNTs, the continuum models are hardly applicable for direct dynamic simulations at a mesoscopic level. A fully three-dimensional dynamic simulation of a nanotube represented by the finite element method[22] can be computationally as expensive as an atomistic MD simulation.

In this paper we present a mesoscopic model capable of simulating systems containing multiple interacting CNTs with modest computing requirements. The model provides a coarse-grained description of the dynamic behavior of CNTs and, at the same time, incorporates the essential physics from the finer (atomic) level. The conceptual description of the model that includes coarse-grained descriptions of both CNTs and molecular matrix, is given in Sec. II. Parametrization of the model representation of individual CNTs, based on the results of atomistic MD simulations, is described in Sec. III. The results of mesoscopic dynamic simulations of free motion of individual nanotubes are presented and compared to the predictions of the atomistic simulations in Sec. IV. The capabilities, limitations, and the potential areas of application of the model are briefly outlined in Sec. V.

II. MESOSCOPIC FORCE FIELD (MFF) MODEL FOR CNTs

In this section we provide a general description of a mesoscopic model designed to describe the dynamic behavior of individual CNTs, the collective dynamics of multiple CNTs, and interaction of CNTs with an organic matrix. The combination of the mesoscopic representation of CNTs with existing coarse-grained models for molecular systems and polymers[23–26] provides a general computational framework for the dynamic simulations of CNT-polymer nanocomposites at time and length scales that are not accessible to either atomistic or continuum computational methods. Practical application of the model to nanocomposites, though, has to be preceded by a careful parametrization of CNT-polymer interaction performed for particular polymer matrixes.

In the mesoscopic model, each single CNT is modeled as a "breathing flexible cylinder" represented by a variable

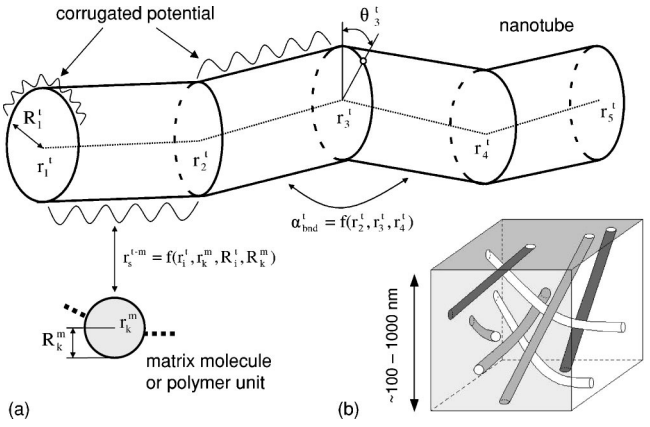

FIG. 1. Schematic representation of a section of nanotube represented by four segments and five nodes (a). The position of *i*th node in the nanotube ($\vec{r}_i^{\,t}$), the radius of the nanotube at node i (R_i^t), and the torsion angle at node i (θ_i^t), are the independent variables that describe the behavior of the nanotube. The sizes of the nanotube, matrix molecule, and the amplitude/period of the corrugated potential are not shown to scale. The model can be used in mesoscopic simulations of collective dynamics of nanotubes in a matrix (b).

number of segments, as shown schematically in Fig. 1(a). The segments are defined by a set of nodes that are located along the nanotube axis, with the length of each segment defined as the length of the nanotube section between two adjacent nodes. The segment length can vary along the nanotube depending on the local transverse curvature. The degrees of freedom, for which equations of motion are solved in dynamic simulations, are the nodes defining the segments, the local radii of the cylinder at the cross sections through the nodes, and the torsion angles at the nodes. The internal interactions within the nanotube are described through a MFF consisting of terms for stretching, bending, torsion, radial breathing, and the coupled stretching-bending, stretching-torsion, and stretching-breathing interactions. This description allows one to reproduce deformation of nanotubes under complex loading conditions that can be realized in a nanocomposite material during processing or under dynamic or static loading conditions.

A general formulation of the model for CNT-polymer nanocomposites can be based on the following Lagrangian L, which describes the system of interacting CNTs and matrix molecules/polymer units:

$$
\begin{aligned}
L = {} & \frac{1}{2}\sum_i m_i^t\left(\frac{dr_i^t}{dt}\right)^2 + \frac{1}{2}\sum_k m_k^m\left(\frac{dr_k^m}{dt}\right)^2 + \frac{1}{2}\sum_i M_i^t\left(\frac{dR_i^t}{dt}\right)^2 \\
& + \frac{1}{2}\sum_k M_k^m\left(\frac{dR_k^m}{dt}\right)^2 + \frac{1}{2}\sum_i M_i^\theta\left(\frac{d\theta_i^t}{dt}\right)^2 - \sum_i U_i^{str} - \sum_i U_i^{bnd} \\
& - \sum_i U_i^{R^t} - \sum_i U_i^{\theta} - \sum_i U_i^{str\text{-}R^t} - \sum_i U_i^{str\text{-}bnd} - \sum_i U_i^{str\text{-}\theta} \\
& - \sum_{i,k} U_{ik}^{t\text{-}m} - \sum_{i,k} U_{ik}^{t\text{-}m(bond)} - \sum_{ij} U_{ij}^{t\text{-}t} - \sum_{kl} U_{kl}^{m\text{-}m} \\
& - \sum_{kl} U_{kl}^{m\text{-}m(bond)} - \sum_k U_k^{R^m}, \qquad (1)
\end{aligned}
$$

where r_i^t is the position of ith node in a nanotube, r_k^m is the position of kth unit of the matrix, R_i^t is the radius of the nanotube at node i, R_k^m is the radius of matrix unit k, θ_i is the torsion angle at node i, $m_i^t=(m_{i-1,i}+m_{i,i+1})/2$ is the mass of a part of the nanotube, represented by the node i, $m_{i,i+1}$ is the mass of the segment $\{i,i+1\}$ of the nanotube located between nodes i and $i+1$, m_k^m is the mass of the kth unit of the matrix, M_i^t and M_k^m are the inertia parameters[25] of the internal breathing motion of the nanotube at node i and matrix unit k, respectively, M_i^θ is the inertia parameter for the twisting motion of the nanotube. The potential energy of the system is composed of terms describing the internal energy of nanotubes ($U^{str}, U^{bnd}, U^{Rt}, U^{\theta}, U^{str\text{-}R}, U^{str\text{-}bnd}, U^{str\text{-}\theta}$), bonded ($U^{m\text{-}m(bond)}$) and nonbonded ($U^{m\text{-}m}$) interaction among the matrix units, bonded and nonbonded interaction among the nanotubes and matrix units ($U^{t\text{-}t}, U^{t\text{-}m}, U^{t\text{-}m(bond)}$), and internal breathing motion of the matrix units (U^{Rm}). In particular, U^{str} is the internal stretching potential defined as a function of the axial deformation of the nanotube segments; U^{bnd} is the bending potential defined as a function of the local curvature of the nantotube segments; U^{Rt} is the internal breathing potential defined as a function of the local radii R_i^t at each node i along the nanotube; U^{θ} is the torsion term defined as a function of the torsional deformation of nanotube; $U^{str\text{-}R}$ and $U^{str\text{-}bnd}$ are the potential energy terms that describe coupling between stretching of two segments adjacent to a node, radial contraction at the node and local curvature at the node; $U^{t\text{-}m}$ is the potential for nonbonded van der Waals interaction between matrix molecules and nanotubes; $U^{t\text{-}m(bond)}$ describes the bonded interaction between matrix molecules and nanotubes due to the formation of chemical bonds; $U^{m\text{-}m}$ and $U^{m\text{-}m(bond)}$ describe the nonbonded and bonded interactions among the matrix units; and U^{Rm} is the internal breathing potential[25] for the matrix units.

The functional forms of the potentials can be chosen based on the results of experimental investigations and/or atomic-level simulations. In particular, data on the vibrational dynamics of the low-frequency modes of the nanotubes (longitudinal stretching, radial breathing, transverse flexion, and torsional twist)[2,5,20,27] as well as available data on the mechanical response of an individual CNT to external loading, such as stress-strain dependence for stretching, bending, and twisting of nanotubes,[2,5,9,10,16,27–30] can be used to find the force constants in the corresponding terms of the internal force field that controls the dynamics of the nanotube. Analytical functions can be used at small deformations, whereas tabulated values of energies and forces can be used to describe complex behavior at large deformations.

The nonbonding interaction among the nanotubes and matrix units, $U^{t\text{-}m}$ and $U^{t\text{-}t}$, is described by a corrugated potential field, as schematically shown in Fig. 1(a), whereas stronger chemical crosslinks between polymer groups and CNTs are included explicitly into the force field. The corrugated potential does not allow the dynamic elements of the model to roll over one another without slipping. Parametrization of the corrugated potential based on the results of atomistic simulations is currently pursued. The equilibrium distances in the interaction potentials $U^{m\text{-}m}, U^{t\text{-}m}, U^{t\text{-}t}$, and $U^{t\text{-}m(bond)}$ are defined in terms of the distances between the edges/surfaces

of the nanotubes and matrix units, e.g., $r_s^{t\text{-}m}$ in Fig. 1(a), rather than their centers. Earlier, this description has been implemented in a mesoscopic model used for simulation of laser ablation of multicomponent organic systems.[25,26] This choice of equilibrium distance is based on the physical concept that the dynamic behavior and cohesion in a nanocomposite is governed primarily by the interaction among atoms on the outside of macromolecules or CNTs (single- or multiwalled) and allows an easy means of simulating complex multicomponent systems, such as nanocomposites containing CNTs and molecules of different sizes.

Once the potential energy of the system is defined, the equations of motion for the five sets of independent variables in the system $\{q\}=\{\vec{r}_i^{\,t},\vec{r}_k^{\,m},R_i^t,R_k^m,\theta_i\}$ can be directly obtained from the Lagrangian given by Eq. (1), as

$$\frac{d}{dt}\frac{\partial L}{\partial \dot{q}_i}-\frac{\partial L}{\partial q_i}=0. \tag{2}$$

The equations of motion for the independent variables can be integrated and classical trajectories can be obtained in a manner similar to the traditional molecular dynamics technique. The trajectories provide complete information on the dynamics of the nanotubes and the matrix molecules at the mesoscopic length scale. A search for the equilibrium molecular/CNT configurations can be performed by the Metropolis Monte Carlo method, in which the potential energy calculation is used to generate a sequence of configurations with probabilities defined by a desired statistical-mechanics distribution. A significant advantage of the MFF model described above is that it does not require an explicit representation of the surface of the nanotube. Rather, the distances between the "virtual surfaces" of the dynamic elements of the model are calculated "on the fly," only when needed to define a particular external interaction. This representation of the shapes of the dynamic elements in the model drastically reduces the number of the independent degrees of freedom and increases computational efficiency of the model.

The first tests of the MFF dynamics model reported in this paper are done for individual nanotubes and the initial parametrization of the terms responsible for the free motion of a nanotube is based on the results of atomistic MD simulations as discussed in Sec. III. An advantage of using a single set of atomistic MD simulations in parametrization of the model is the ability to directly compare the predictions of the mesoscopic and fully atomistic models. The comparison of the dynamic behavior of individual nanotubes represented at the atomic and mesoscopic levels is reported in Sec. IV and is used to analyze the capabilities and limitations of the mesoscopic model.

III. PARAMETRIZATION OF MFF FOR AN INDIVIDUAL CNT FROM ATOMISTIC MD SIMULATIONS

The functional form and force field parameters for the stretching, bending, and torsion contributions to the mesoscopic force field [Eq. (1)] are determined in a series of quasistatic atomic-level MD simulations performed with semiempirical many-body Brenner interatomic potential.[31] The atomistic simulations are performed for nine nanotubes of different radii; namely, (5,0), (5,5), (10,0), (15,0), (10,10), (20,0), (25,0), (15,15), (30,0). The results of the atomistic simulations and corresponding terms of the mesoscopic force field are described below.

A. Stretching term of the MFF

In the simplest linear (harmonic) approximation, the internal stretching potential, U^{str}, is defined as a function of the axial deformation of nanotube segments:

$$U^{str}=\sum_{i=1}^{N-1}L_{i,i+1}^0\frac{1}{2}k_{str}\varepsilon_{i,i+1}^2=\sum_{i=1}^{N-1}L_{i,i+1}^0\frac{1}{2}k_{str}\left(\frac{L_{i,i+1}-L_{i,i+1}^0}{L_{i,i+1}^0}\right)^2, \tag{3}$$

where $L_{i,i+1}^0$ is equilibrium (unstrained) length of a segment between i and $i+1$ nodes of the mesoscopic representation of the nanotube, $L_{i,i+1}$ is current length of the segment between i and $i+1$ nodes that can be expressed through the positions of the nodes, $L_{i,i+1}=|\vec{r}_{i+1}^{\,t}-\vec{r}_i^{\,t}|$, $\varepsilon_{i,i+1}$ is local axial strain of the segment, and k_{str} is stretching force constant.

In order to determine the values of the stretching force constant, we perform a series of atomistic simulations for nanotubes of different radii. A periodic boundary condition in the direction of the tube axis is used to simulate stretching of infinitely long isolated nanotubes. Computational cells containing two and three CNT unit cells are used in simulations of armchair (n,n) and zigzag $(n,0)$ nanotubes, respectively. The axial strain is applied by changing the size of the computational cell along the nanotube axis and performing energy minimization by simulated annealing. Here and in other energy minimization simulations described below, the time of the simulated annealing is chosen to ensure that the total energy of the system does not change by more than 0.001 eV during the last 100 ps of the simulations. Simulations at four values of the axial strain, -0.02, -0.01, 0.01, and 0.02, are performed and the force constants are calculated through the second derivative of the strain energy with respect to the axial strain. The results of the calculations are shown in Fig. 2(a). For nanotubes with radii larger than $\sim$4 Å, the dependence of the stretching force constant (in eV/Å) on the equilibrium radius of the nanotube R_{eq}^r (in Å) can be relatively well described by a linear dependence, as

$$k_{str}=86.64+100.56R_{eq}^r. \tag{4}$$

For nanotubes with radii larger than 4 Å, the values of the force constant expressed in units of energy per atom are essentially independent of the radius and chirality of the nanotube and fall within 2 eV/atom range around the average value of 46.8 eV/atom. Somewhat higher values of 52.0 and 51.7 eV/atom are calculated for (5,5) and (5,0) nanotubes having radii of 3.44 and 2.07 Å, respectively. The force constants for the small radius nanotubes expressed in energy per unit length [Fig. 2(a)], are smaller as compared to the larger radius nanotubes. This is related to a more significant elongation of the small-radius nanotubes during the initial structural relaxation performed with fully atomistic MD. The results on the stretching force constants reported above are in

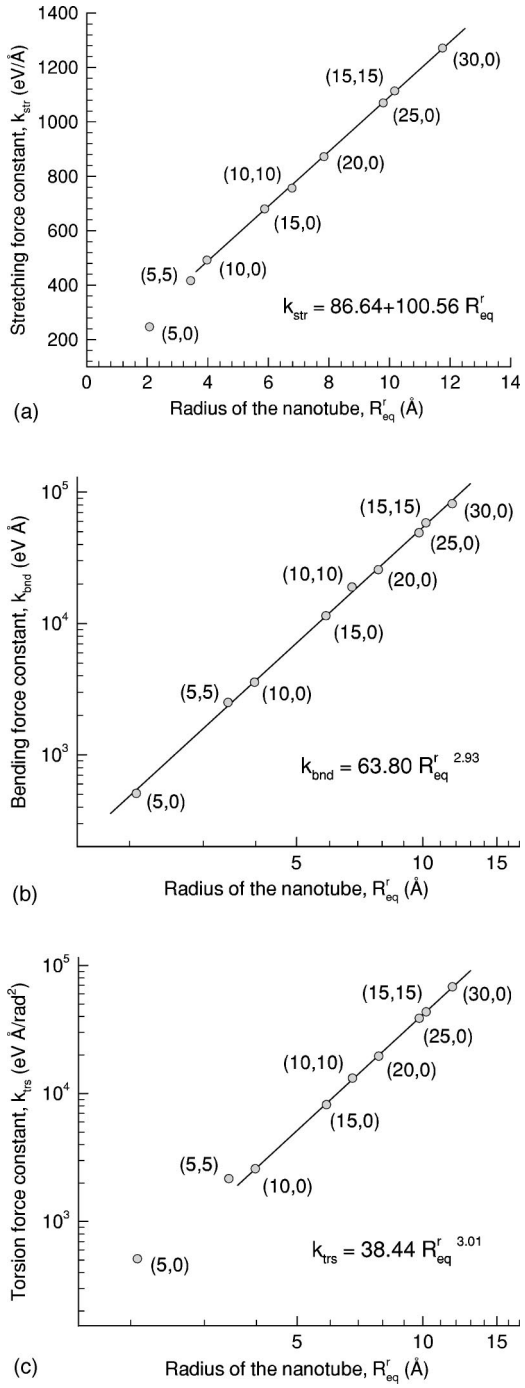

FIG. 2. Force constants of the stretching, bending, and torsion energy terms of the mesoscopic force field determined from a series of quasistatic atomistic simulations performed with Brenner interatomic potential for nanotubes of different radii. Lines correspond to linear (a) and power law (b,c) fits of the data points, with corresponding expressions shown in the figures.

good agreement with earlier calculations performed with Brenner potential[32] as well as with *ab initio* calculations based on the local density approximation to the density functional theory.[27] The values of ~ 59 eV/atom[32] and ~ 56 eV/atom[27] are reported in these works for the stretching force constants. Note that the purpose of the atomistic simulations reported in this work is not to verify or confirm the results reported earlier, but to provide a consistent parametrization of different terms of the MFF described by Eq. (1).

The calculation of the stretching force constant discussed above is performed for a small range of the axial strain, from -0.02 to 0.02, in which no deviations from the quadratic dependence of the strain energy on strain is observed. It is known that buckling of CNTs at large compressions or formation of Stone-Wales rotation defects at large tensile stresses leads to a drop in the stiffness of the nanotube. These effects can be incorporated into the MFF as needed by defining switching functions and criteria for transition between different regimes of nanotube deformation. As the model is aimed mainly at large-scale phenomena, local changes in shapes of the nanotubes associated with nonlinear behavior at large deformations are not expected to play a major role and representation of CNTs as cylinders may still remain valid in the nonlinear elastic/plastic regime.

B. Bending term of the MFF

The internal bending potential U^{bnd} is defined as a function of the curvature of nanotube segments:

$$U^{bnd} = \frac{1}{2}k_{bnd}\sum_{i=1}^{N-1} L^0_{i,i+1}\left(\frac{1}{R^{curv}_{i,i+1}}\right)^2 \approx \frac{1}{2}k_{bnd}\sum_{i=2}^{N-1}\left\{\frac{1}{2}L^0_{i,i-1}\left(\frac{1}{R^{curv}_{i}}\right)^2 + \frac{1}{2}L^0_{i,i+1}\left(\frac{1}{R^{curv}_{i}}\right)^2\right\}, \quad (5)$$

where $L^0_{i,i+1}$ is equilibrium (unstrained) length of the segment between i and $i+1$ nodes, $R^{curv}_{i,i+1}$ is radius of curvature of the segment defined by the i and $i+1$ nodes, R^{curv}_i is radius of curvature at node i, and k_{bnd} is the bending force constant.

Similar to the stretching force constant discussed above in Sec. III A, the values of the bending force constant are determined in a series of atomistic simulations performed for nanotubes of different radii. Larger computational cells containing 13 unit cells for armchair nanotubes and 15 unit cells for zigzag nanotubes were used in the simulations. No periodic boundary conditions are applied in the simulations. The CNTs are initially bent with a constant radius of curvature that is varied between 22 528 and 4528 Å (corresponding to the bending angles from 0.0025 to 0.0127 deg/Å). The bent nanotubes are then allowed to relax for 1.5 ns in annealing simulations performed with the end segments fixed. The force constants are calculated through the second derivative of the strain energy with respect to the curvature, and the results of the calculations are shown in Fig. 2(b). The dependence of the bending force constant (in eV Å) on the equilibrium radius of the nanotube (in Å) can be described by a power law fit, yielding the following expression:

$$k_{bnd} = 63.80 R^{r\ 2.93}_{eq}, \quad (6)$$

which is close to the cubic dependence of the bending force constant on the radius expected for an elastic tube.

The calculated bending stiffness is in good agreement with the values obtained from tight-binding simulations, in which the values of 2.08×10^4 and 1.95×10^4 eV Å are reported for (10,10) and (12,8) CNTs, respectively.[33] The bend-

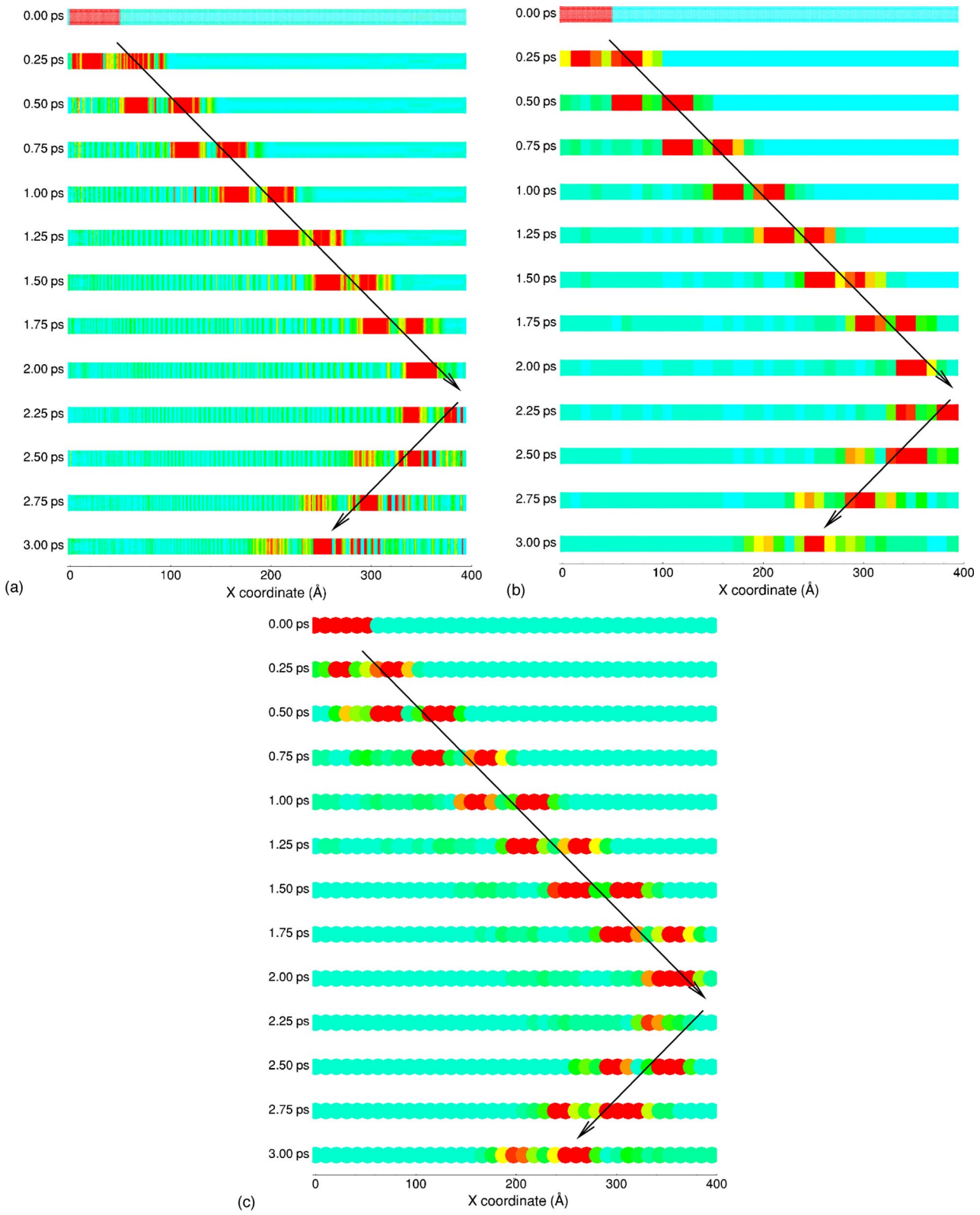

FIG. 3. (Color online) Strain energy distributions in atomistic (a,b) and mesoscopic (c) simulations of an acoustic wave propagation in a 395 Å long (10,10) CNT. The value of the strain energy density is shown by the color scale: light blue (light gray in print gray-scale version) color corresponds to zero energy, red (dark gray in print gray-scale version) color corresponds to the energy density of 0.002 eV/atom. In the atomistic simulation, the distribution of the strain energy at atomic level is shown in (a) and the energy averaged over ~1 nm long segments defined in the mesoscopic model is shown in (b). The nanotube is represented by 39 nodes in the mesoscopic model and by 6440 atoms in the atomistic MD model. Arrows show schematically the paths of the acoustic wave.

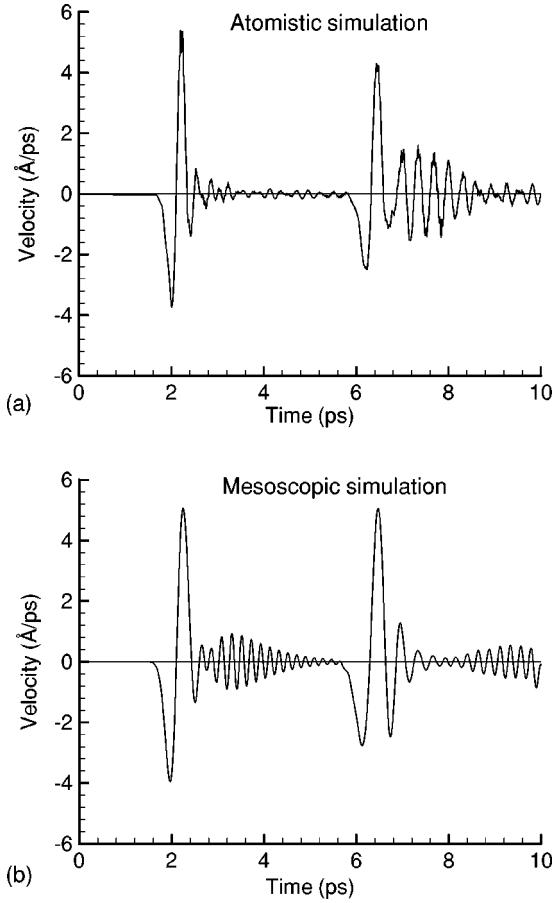

FIG. 4. Velocity of the far (right) end part of a 395 Å long (10,10) CNT in atomistic (a) and mesoscopic (b) simulations of an acoustic wave propagation, illustrated in Fig. 3. In the atomistic simulation, the velocity is averaged over atoms that belong to the ~1 nm long end segment of the CNT, in the mesoscopic simulation the velocity of the end node is plotted.

ing force constant of 1.90×10^4 eV Å is measured for (10,10) CNT in our MD simulations performed with empirical Brenner potential.

Nonlinear elastic phenomena, such as rippling[34,35] or buckling[16,29] of CNTs at large bending angles, can substantially reduce the effective bending stiffness of the nanotube. The effect of nonlinear bending deformation can be incorporated into the MFF as needed by defining switching functions and criteria for transition between different regimes of nanotube deformation. The calculation of the bending force constant discussed above was performed for a small range of bending angles for which no deviation from the quadratic dependence of the strain energy on curvature is observed.

C. Torsion term of the MFF

The torsion term in the MFF (U^θ) is defined as a function of the torsional deformation of nanotube segments:

$$U^\theta = \sum_{i=1}^{N-1} L^0_{i,i+1} \frac{1}{2} k_t \left(\frac{\theta_i - \theta_{i+1}}{L^0_{i,i+1}} \right)^2, \tag{7}$$

where θ_i is torsion angle at node i and k_t is torsion force constant.

The values of the torsion force constant are determined in a series of atomistic simulations performed for nanotubes of different radii. Computational cells of the same size as in bending simulations described above are used in the simulations. The CNTs are initially twisted with a constant torsional deformation along the nanotube, which was varied between 0.0025 to 0.0127 deg/ Å. The twisted nanotubes are then allowed to relax for 1 ns in annealing simulations performed with the end segments fixed. The force constant calculated through the second derivative of the strain energy with respect to the torsional deformation is shown in Fig. 2(c). For nanotubes with radii larger than ~4 Å, the dependence of the torsion force constant (in eV Å/rad^2) on the equilibrium radius of the nanotube (in Å) can be described by a power law fit, yielding the following expression:

$$k_{trs} = 38.44 R_{eq}^{r\ 3.01}, \tag{8}$$

which is close to the cubic dependence on the radius expected for a twisted hollow cylinder.

The torsion force constant of 1.3×10^4 eV Å/rad^2 calculated in this work for (10,10) CNT is in a reasonable agreement with values obtained in tight-binding simulations, 1.73×10^4 eV Å/rad^2 for a (10,10) CNT, and 1.46×10^4 and 1.63×10^4 eV Å/rad^2 for left and right twists of a (12,8) CNT, respectively.[33]

Large torsional deformations of CNTs can lead to deviations from the linear elastic response, e.g., buckling of a twisted (10,10) CNT has been reported in a computational study[34] at a shear strain of 5%. Similar to the nonlinear behavior in stretching and bending deformations, the effect of nonlinear torsional deformation can be incorporated into the MFF if large deformations are expected to take place in the simulations.

IV. FREE VIBRATIONS OF INDIVIDUAL CNTs: MESOSCOPIC AND ATOMISTIC SIMULATIONS

As a first test of the mesoscopic model and the parametrization described above, we perform a series of simulations of a free motion of a single-walled CNT with both the mesoscopic and fully atomistic MD models. The initial conditions in the simulations are chosen to provide targeted testing of the two terms of the MFF discussed above; stretching and bending. The torsion angle in the mesoscopic model is only weakly coupled to other independent variables through the torsion-stretching coupling term. As a result, torsional motion of an isolated nanotube is trivial and is not discussed in this paper. The role of the radial breathing term and the coupling terms in the Lagrangian [Eq. (1)] is to provide a higher order of accuracy in the description of the dynamic behavior of CNTs and to facilitate the energy transfer between different modes during motion. A direct comparison between the results of the mesoscopic and atomistic simulations described below suggests that the omission of these terms has a relatively minor effect on the dynamic behavior of the mesoscopic representation of an individual CNT. For some of the potential applications of the model, however, high accuracy in the dynamic behavior of the model may be essential, and fine tuning of the mesoscopic force field through the

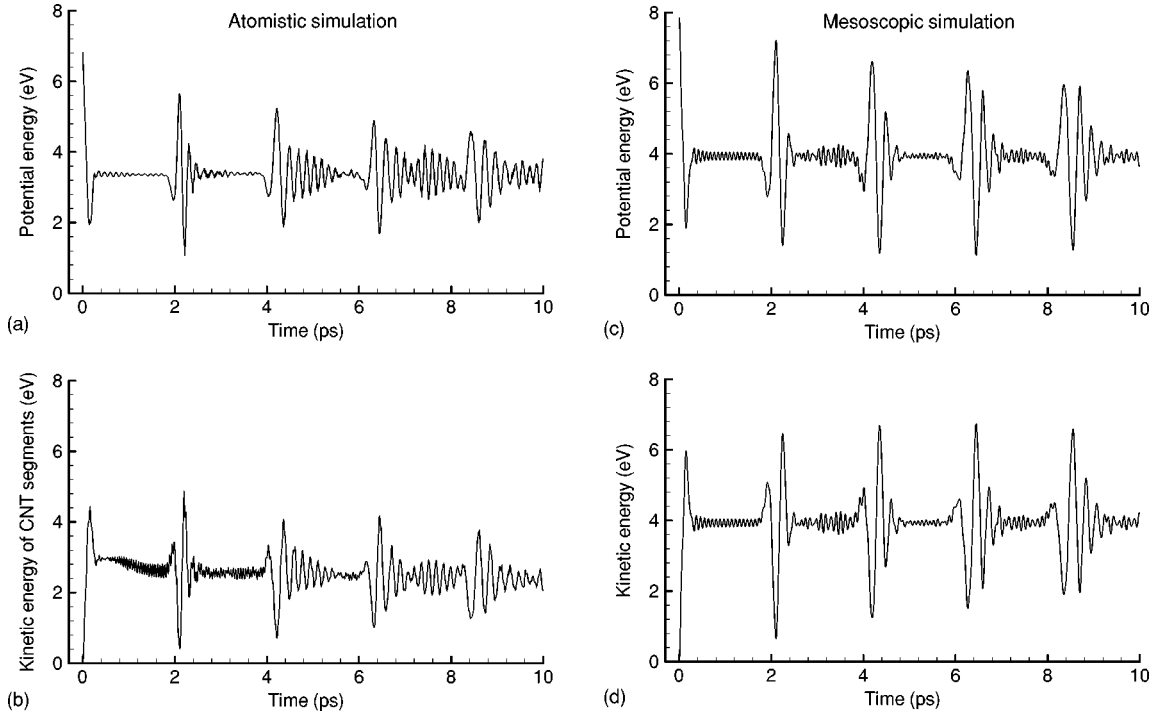

FIG. 5. Time dependence of the potential energy and kinetic energy of a 395 Å long (10,10) CNT in atomistic (a,b) and mesoscopic (c,d) simulations of an acoustic wave propagation, illustrated in Fig. 3. The potential energy is shown relatively to the potential energy of a relaxed CNT and corresponds to the strain energy due to the wave. In the atomistic simulation, the kinetic energy is calculated as a sum of kinetic energies of the center-of-mass motion of 38 ~1 nm long CNT segments and does not include the energy of the high-frequency thermal atomic motions in the center-of-mass reference frame.

coupling terms may be required. Therefore, we retain the coupling terms in the general formulation of the model, given in Eq. (1).

A. Acoustic wave propagation

Acoustic wave propagation is simulated in a 395 Å long (10,10) CNT represented with MFF and atomistic models. The wave is generated by creating a local tensile strain of 2% in a ~50 Å end part of the CNT (left end in Fig. 3) at the beginning of the simulations and allowing the systems to evolve freely at later times. In the atomistic MD simulation the (10,10) CNT is represented by 6400 carbon atoms and 40 hydrogen atoms. The hydrogen atoms are used at the ends of the nanotube (20 atoms at each end) to terminate dangling bonds and to ensure stability of the nanotube. The interatomic interaction is described by the Brenner potential for hydrocarbons, which is the potential used to deduce the MFF as described in Sec. III. In the MFF model, the CNT is represented by 38 segments connecting 39 nodes, with each segment having equilibrium length $L^0_{i,i+1}$ of ~10.4 Å and a mass $m_{i,i+1}$ of 2022 amu, $i=1, \ldots, 38$.

A visual picture of the acoustic wave propagation is given in Fig. 3, where the evolution of the strain energy is shown for different times during the simulations. The strain energy distributions in the atomistic MD simulations are shown with atomic-level resolution in Fig. 3(a). It can be seen that initially there is a uniform local strain energy distribution in the strained left end of the CNT. As time progresses, the relaxation of the initial tensile stresses in the left part of the nanotube leads to the formation of a bimodal stress wave that propagates through the nanotube. The wave consists of a tensile component that propagates first and a compression component that follows. The bimodal structure of the wave is a result of the interaction of the initial tensile stresses with the free surface. Both the tensile and compression components of the wave show up in Fig. 3 as red regions of high strain energy separated by a light blue/green band that corresponds to the transition from expansion to compression. By ~2 ps, the acoustic wave reaches the far (right) end of the nanotube and reflects back. Upon reflection, the stress wave changes sign (the compression component now leads and the tensile component follows). While one can notice from the figure that there is some dissipation of the energy of the wave with time, the wave packet still contains the largest fraction of the initial strain energy and can be clearly identified at all times during the simulation.

A mesoscopic simulation performed for the same initial conditions as the atomistic one is illustrated in Fig. 3(c). In order to quantitatively compare the results of the mesoscopic and atomistic simulations, the same color scale is used to show the energy density in both simulations, from light blue color corresponding to zero energy, to red color corresponding to 0.002 eV/atom. Moreover, an alternative representation of the potential energy distribution in the atomistic simulation, in which the potential energy is averaged over atoms that belong to segments of the nanotube of the same size as in the mesoscopic model, is shown in Fig. 3(b). Fine details at the atomic level that can be observed in Fig. 3(a)

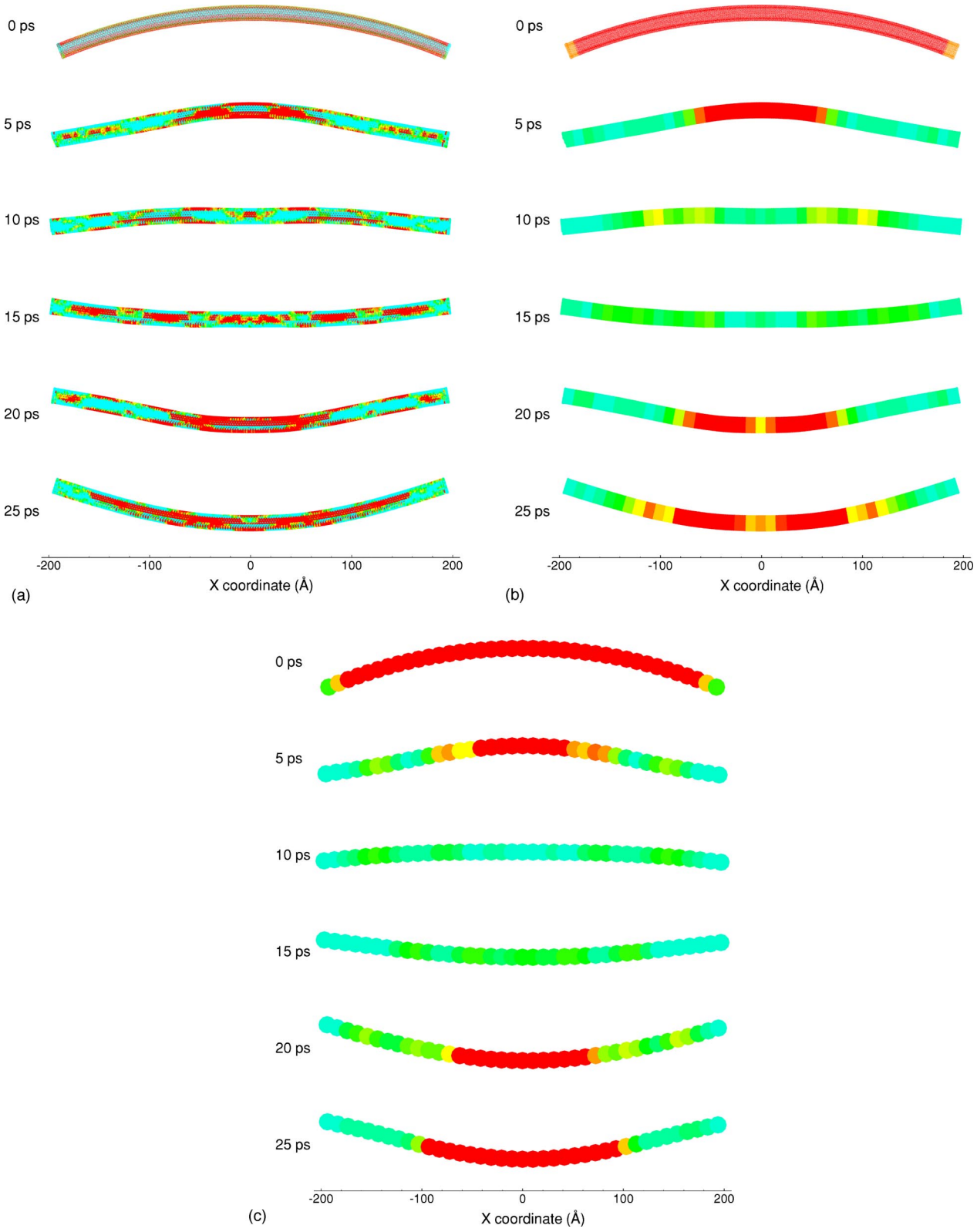

FIG. 6. (Color online) Strain energy distributions in atomistic (a,b) and mesoscopic (c) simulations of free bending vibrations of a 395 Å long (10,10) CNT with the initial radius of curvature equal to 500 Å. The value of the strain energy density is shown by the color scale: light blue (light gray in print gray-scale version) color corresponds to zero energy, red (dark gray in print gray-scale version) color corresponds to the energy density of 0.002 eV/atom. In the atomistic simulation, the distribution of the strain energy at atomic level is shown in (a) and the energy averaged over ~1 nm long segments defined in the mesoscopic model is shown in (b). The nanotube is represented by 39 nodes in the mesoscopic model and by 6440 atoms in the atomistic MD model.

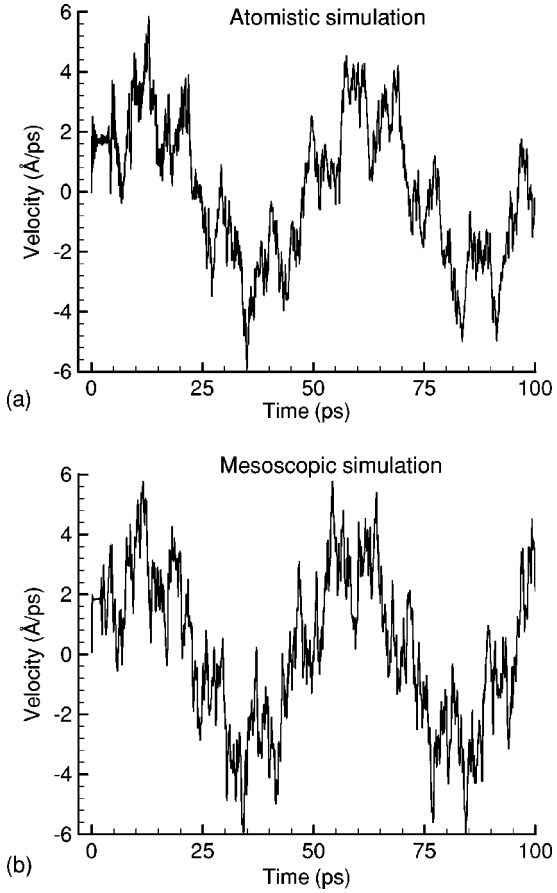

FIG. 7. Velocity of an end part of a 395 Å long (10,10) CNT in atomistic (a) and mesoscopic (b) simulations of free bending vibrations, illustrated in Fig. 6. In the atomistic simulation, the velocity is averaged over atoms that belong to a ~1 nm long end segment of the CNT, in the mesoscopic simulation the velocity of an end node is plotted.

are smeared out in Fig. 3(b), making the comparison between the atomistic and mesoscopic simulations easier. Both the velocity of the wave and characteristic features of the strain energy distributions in Figs. 3(b) and 3(c) show good agreement.

Plots of the velocities of the far (right) ends of the nanotubes, given in Fig. 4, allow for a more detailed quantitative comparison between the atomistic and mesoscopic simulation results. There is a good match in the overall shape of the plots and in the amplitudes of the velocity spikes that correspond to the reflections of the wave packet from the far end of the nanotube. The structure of the velocity spike agrees with the notion of the bimodal wave interacting with a free surface: the tensile component of the wave arrives first, pulling the end part of the nanotube in the negative direction (negative part of the velocity spike); the compressive component follows, pushing the end part of the nanotube back (positive part of the velocity spike).

The time evolution of the total potential and kinetic energies of the nanotube during the simulations is shown in Fig. 5. In both atomistic and mesoscopic simulations all energy is initially stored in the potential energy of the stretched part of the nanotube. As the acoustic wave develops, the energy partition about evenly between the potential and kinetic energy of the wave. To make a comparison to the mesoscopic simulation, the kinetic energy shown in Fig. 4(b) is defined as the kinetic energy of the collective center-of-mass motion of the CNT segments equivalent to the ones in the mesoscopic model. This kinetic energy does not include the energy of the radial breathing mode as well as the thermal energy of the high-frequency atomic motions in the center-of-mass reference frame. The spikes in the plots of the potential and kinetic energies correspond to the reflections of the wave from the ends of the nanotube and the time between the spikes can be used to estimate the speed of the wave: ~18 000 m/s. In both atomistic and mesoscopic simulations, the wave gradually dissipates upon multiple reflections, although the dissipation is more pronounced in the atomistic simulation, where a larger number of vibrational modes and anharmonicity of interatomic interaction potential result in a faster energy dissipation. Apart from the thermal energy that is not included in the mesoscopic model, a quantitative difference in the levels of the potential [Figs. 5(a) and 5(c)] and kinetic energies [Figs. 5(b) and 5(d)] is related to the difference in the initial energy of the stretched configurations (starting points in the potential energy plots at $t=0$). The total energy of the three segments (total length of ~52 Å) stretched by 2% in the mesoscopic simulation is 7.87 eV, whereas the initial energy in the atomistic simulation is somewhat lower: 6.3 eV.

Overall, we can conclude that the mesoscopic model reproduces well most of the characteristics of the acoustic wave propagating in a CNT. A major advantage of the mesoscopic description of the nanotube dynamics is the low computational cost of the simulations. The atomistic simulation of 10 ps trajectory of the CNT shown in Fig. 3 took 21 h on a dedicated SGI Origin 3800 workstation, whereas the mesoscopic simulation took less than a tenth of a second on a desktop PC.

B. Free bending vibrations

To additionally test the mesoscopic model, a simulation of free vibrations of a bent (10,10) CNT has been simulated and compared to the results of atomistic simulations. The same system as in the study of the acoustic wave propagation, a 395 Å long (10,10) CNT, is used in the simulations. The CNT is initially bent with a constant radius of curvature, $R^{curv}=500$ Å, along the whole length of the CNT and then, starting at a time of 0 ps, is allowed to evolve freely in the atomistic and mesoscopic simulations.

Snapshots from the simulations of free motion of the CNT are shown in Fig. 6. The color distribution corresponds to the local potential energy density at various times. The strain energy is shown with atomic-level resolution in Fig. 6(a) and is averaged over nanotube segments in Fig. 6(b). It can be seen that initially there is a uniform strain energy distribution in the CNT. The relaxation of the CNT can be described as propagation of two unloading waves that start from the end parts of the CNT and propagate towards the center. The CNT then undergoes free bending vibrations with characteristic frequency of 21 GHz in the atomistic simulation and 20 GHz

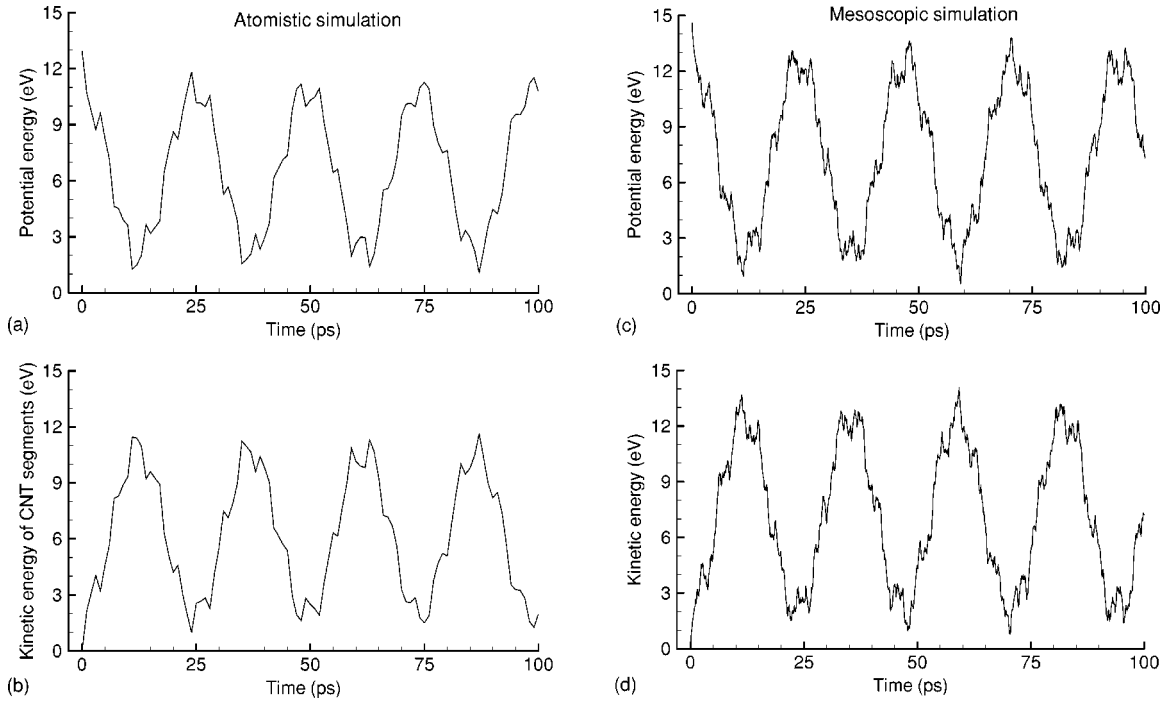

FIG. 8. Time dependence of the potential energy and kinetic energy of a 395 Å long (10,10) CNT in atomistic (a,b) and mesoscopic (c,d) simulations of free bending vibrations, illustrated in Fig. 6. The potential energy is shown relatively to the potential energy of a relaxed CNT and corresponds to the strain energy due to the bending vibrations. In the atomistic simulation, the kinetic energy is calculated as a sum of kinetic energies of the center-of-mass motion of thirty-eight ~1 nm long CNT segments and does not include the energy of the high-frequency thermal atomic motions in the center-of-mass reference frame.

in the mesoscopic simulation. The discrepancy in the frequency of the bending vibrations can be attributed to the deviation from the linear regime (quadratic dependence of the strain energy on curvature, assumed in the parametrization of the bending force constant, Sec. III B) at high bending angles realized in the simulations shown in Fig. 6. Indeed, the bending angles up to 0.0025 deg/Å were used in parametrization of the MFF, much below the bending angle of 0.1146 deg/Å that corresponds to $R^{curv}=500$ Å. This minor discrepancy can be fixed by adapting an anharmonic potential fitted to the data from atomistic simulations in a wider range of bending angles.

In order to perform a more detailed quantitative comparison of the dynamics of the bending vibrations predicted by the atomistic and mesoscopic models, velocities of the end parts of the CNTs are plotted in Fig. 7. Apart from a slightly higher vibrational frequency in the mesoscopic simulation, the agreement between the two simulations is remarkable. The velocity plots show a very good match not only in the overall shapes but also in the detailed vibrational structure of the trajectories.

The time dependence of the kinetic and potential energies during the simulations is shown in Fig. 8. Initially, all the energy is stored in the potential energy of the bent configurations. The initial potential energy in the mesoscopic simulation [Fig. 8(a)] is 14.6 eV, somewhat lower than 15 eV predicted by the first part of Eq. (5). The discrepancy is related to zero bending energy associated with the end nodes in the mesoscopic model. An increase in the number of nodes representing the nanotube brings the initial bending energy closer to 15 eV. A lower value of the initial energy in the atomistic configuration is related to the deviation from the linear regime at high bending angles discussed above. During the simulations, the energy is partitioned between the potential and kinetic energies. In the mesoscopic simulation a small part of the energy is leaking into the stretching energy through the inertial coupling (the term of the MFF responsible for the explicit coupling between stretching and bending is not activated in this simulation). The stretching contribution to the potential energy does not exceed 1% of the total potential energy during the simulation. Similar to Fig. 5(b), the kinetic energy shown in Fig. 8(b) is defined as kinetic energy of the collective center-of-mass motion of the CNT segments equivalent to the segments in the mesoscopic model. The energy of the atomic motions in the center-of-mass reference frame, excluded in this definition, increases during the first several picoseconds of the simulation to ~0.15 eV (~1.1% of the total energy) and then slowly increases up to ~0.2 eV (2.3% of the total energy) during the time of the simulation, 100 ps.

Similar to the stretching simulations, we can conclude that the bending vibrations of an individual nanotube can be well represented by the mesoscopic model for a tiny fraction of the computational cost. The 100 ps atomistic simulation of bending vibration took more than a week of calculations on a dedicated SGI Origin 3800 workstation, whereas the corresponding mesoscopic simulation took less than 1 second on a desktop PC.

V. DISCUSSION AND SUMMARY

The principal challenge in the computational modeling of nanostructures and nanocomposites based on carbon nanotubes is presented by the gap between the atomistic description of individual nanotubes and the collective behavior and properties of large groups of CNTs in nanocomposite materials or nanostructures. While atomistic simulations can provide detailed information on the behavior of individual CNTs, the calculations are computationally expensive and difficult to extend to systems containing multiple CNTs. In this paper we present a coarse-grained force-field model for CNTs that provides a computationally efficient description of CNTs and can help to close the gap between the atomistic and continuum descriptions of CNT-based materials and structures. The coarse-grained (or mesoscopic) model incorporates the essential information from the atomic-level simulations and represents the dynamic behavior of a CNT with a drastically reduced number of degrees of freedom. Specifically, a CNT is represented as a "breathing flexible cylinder" consisting of a variable number of segments. The surface of the nanotube is not represented explicitly in the model but is calculated from a limited set of dynamic variables only when needed to define a particular external interaction. This representation drastically reduces the number of the independent degrees of freedom and makes the model much more efficient as compared to conventional representations based on continuum mechanics concepts.

First test simulations performed for the acoustic wave propagation and free bending vibrations of the nanotube demonstrate that the mesoscopic model reproduces well the short-term dynamic behavior of individual CNTs as predicted in atomistic simulations. If required for a particular application, a quantitative agreement between the results of mesoscopic and atomistic simulations can be further improved by fine tuning the parameters of the MFF and inclusion of additional terms responsible for coupling between different dynamic degrees of freedom in the model. Moreover, the high-frequency vibrational modes that are not included in the mesoscopic model explicitly can be accounted for by connecting the long-wavelength internal elastic modes with a "heat bath" that represents the remaining degrees of freedom of the CNT. Although the initial parametrization and testing of the mesoscopic model discussed in this paper has been performed for single-walled CNTs, the MFF given by Eq. (1) can be easily applied to multiwalled CNTs, which are often used in polymer-matrix nanocomposites. Similarly to single-walled CNTs, parametrization of the model for multiwalled CNTs can be performed based on the results of atomistic simulations or experimental data on the behavior and properties of multiwalled CNTs.

The main advantage of the mesoscopic model is its high computational efficiency. Simulation of the dynamics of a 395 Å long (10,10) CNT for several periods of bending vibrations took less than a second on a desktop PC, suggesting that mesoscopic simulations of much larger systems containing multiple CNTs and other constituents represented at a mesoscale level (e.g., coarse-grained representation of molecular systems[23–26]) is possible. The length scale of a dynamic simulation is defined by the size of the dynamic elements for which the equations of motion are solved. The dynamic elements in the model are significantly larger than the atoms and the size of the computational cell can also be much larger than the one used in atomistic simulations. The time scale of the simulations is defined by the time step in the numerical integration. Since explicit atomic vibrations are not followed in the model, the time step of integration can be increased by up to several orders of magnitude. Parametrization of the external interactions for CNTs embedded in a polymer matrix and simulation of the CNT-based polymer nanocomposite systems, such as the one shown schematically in Fig. 1(b), is the subject of our current work.

ACKNOWLEDGMENTS

One author (L. V. Z.) gratefully acknowledges financial support provided by the National Science Foundation (DMII-0422632 and NIRT-0403876).

*Corresponding author. Email address: lz2n@virginia.edu
†Email address: cwei@nas.nasa.gov
‡Email address: deepak@nas.nasa.gov

[1] S. Iijima, Nature (London) **56**, 354 (1991).
[2] T. Ebbesen, *Carbon Nanotubes: Preparation and Properties* (CRC Press, Boca Raton, 1997).
[3] E. T. Thostenson, Z. Ren, and T. W. Chou, Compos. Sci. Technol. **61**, 1899 (2001).
[4] S. B. Sinnott and R. Andrews, CRC Crit. Rev. Solid State Mater. Sci. **26**, 145 (2001).
[5] B. I. Yakobson and P. Avouris, Top. Appl. Phys. **80**, 287 (2001).
[6] O. A. Shenderova, V. V. Zhirnov, and D. W. Brenner, CRC Crit. Rev. Solid State Mater. Sci. **27**, 227 (2002).
[7] D. Srivastava, in *Science and Technology of Carbon Nanotubes: Applications Perspective*, edited by M. Meyyappan (CRC Press, Boca Raton, FL, 2004), Chap. 2.
[8] *Polymer nanocomposites*, edited by R. A. Vaia and R. Krishnamoorti (American Chemical Society, Washington, DC, 2001).
[9] D. Srivastava, M. Menon, and K. Cho, Phys. Rev. Lett. **83**, 2973 (1999).
[10] J. W. Che, T. Cagin, and W. A. Goddard, Nanotechnology **10**, 263 (1999).
[11] C. Wei, D. Srivastava, and K. Cho, Phys. Rev. B **67**, 115407 (2003).
[12] D. Srivastava, D. W. Brenner, J. D. Schall, K. D. Ausman, M. F. Yu, and R. S. Ruoff, J. Phys. Chem. B **103**, 4330 (1999).
[13] S. J. V. Frankland, A. Caglar, D. W. Brenner, and M. Griebel, J. Phys. Chem. B **106**, 3046 (2002).
[14] V. Lordi and N. Yao, J. Mater. Res. **15**, 2770 (2000).
[15] C. Wei, D. Srivastava, and K. Cho, Nano Lett. **2**, 647 (2002).
[16] B. I. Yakobson, C. J. Brabec, and J. Bernholc, Phys. Rev. Lett. **76**, 2511 (1996).

[17] S. Govindjee and J. L. Sackman, Solid State Commun. **110**, 227 (1999).
[18] C. Q. Ru, Phys. Rev. B **62**, 9973 (2000).
[19] G. M. Odegard, T. S. Gates, L. M. Nicholson, and K. E. Wise, Compos. Sci. Technol. **62**, 1869 (2002).
[20] K. Sohlberg, B. G. Sumpter, R. E. Tuzun, and D. W. Noid, Nanotechnology **9**, 30 (1998).
[21] V. M. Harik, Comput. Mater. Sci. **24**, 312 (2002).
[22] P. S. Das and L. T. Wille, Comput. Mater. Sci. **24**, 159 (2002).
[23] *Computer Simulation of Polymers*, edited by E. A. Colbourn (Longman Scientific and Technical, New York, 1994).
[24] K. Kremer and F. Müller-Plathe, MRS Bull. **26**, 205 (2001).
[25] L. V. Zhigilei, P. B. S. Kodali, and B. J. Garrison, J. Phys. Chem. B **102**, 2845 (1998).
[26] L. V. Zhigilei, E. Leveugle, B. J. Garrison, Y. G. Yingling, and M. I. Zeifman, Chem. Rev. (Washington, D.C.) **103**, 321 (2003).
[27] D. Sánchez-Portal, E. Artacho, J. M. Soler, A. Rubio, and P. Ordejón, Phys. Rev. B **59**, 12678 (1999).
[28] M. R. Falvo, G. J. Clary, R. M. Taylor, V. Chi, F. P. Brooks, S. Washburn, and R. Superfine, Nature (London) **389**, 582 (1997).
[29] E. W. Wong, P. E. Sheehan, and C. M. Lieber, Science **277**, 1971 (1997).
[30] J.-P. Salvetat, J. M. Bonard, N. H. Thomson, A. J. Kulik, L. Forro, W. Benoit, and L. Zuppiroli, Appl. Phys. A: Mater. Sci. Process. **69**, 255 (1999).
[31] D. W. Brenner, Phys. Rev. B **42**, 9458 (1990).
[32] D. H. Robertson, D. W. Brenner, and J. W. Mintmire, Phys. Rev. B **45**, 12592 (1992).
[33] L. Vaccarini, C. Goze, L. Henrard, E. Hernández, P. Bernier, and A. Rubio, Carbon **38**, 1681 (2000).
[34] M. Arroyo and T. Belytschko, Phys. Rev. Lett. **91**, 215505 (2003).
[35] J. Z. Liu, Q. Zheng, and Q. Jiang, Phys. Rev. Lett. **86**, 4843 (2001).